Key Points:
- Significant discharge from primary channels is allocated to islands
- Travel times within islands are significantly longer than in the channels
- A hydrological connectivity framework is useful for understanding delta systems

Correspondence to:
P. Passalacqua,
paola@austin.utexas.edu

Hydrological connectivity in river deltas: The first-order importance of channel-island exchange

Matthew Hiatt[1] and Paola Passalacqua[1]

[1]Department of Civil, Architectural, and Environmental Engineering, Center for Research in Water Resources, University of Texas at Austin, Austin, Texas, USA

Abstract Deltaic systems are composed of distributary channels and interdistributary islands. While previous work has focused either on the channels or on the islands, here we study the hydrological exchange between channels and islands and point at its important role in delta morphology and ecology. We focus our analysis on Wax Lake Delta in coastal Louisiana (USA) and characterize the surface water component of hydrological connectivity through measurements of water discharge and hydraulic tracer propagation. We find that deltaic islands are zones of significant water flux as 23–54% of the incoming distributary channel flux enters the islands. A calculation of the travel times through a channel-island complex shows travel times through the islands to be at least 3 times their channel counterparts. A dye release experiment also indicates that travel times in islands are much longer that those within channels as dye remained in the island for the 3.8 day duration of the experiment. Additionally, islands are more sensitive than channels to environmental forces such as tides, which cause flow reversal and thus can increase travel times through the islands. Our work defines the "hydrological network" of a river delta to include not only the distributary channel network but also the interdistributary islands, quantifies the implications of channel-island hydrological connectivity to travel times through the system, and discusses the relevance of our findings to channel mouth dynamics at the delta front and the potential for denitrification in coastal systems.

1. Introduction

Hydrological connectivity refers to flows of matter and energy (water, sediment, nutrients, etc.) through different components of a landscape [*Tetzlaff et al.*, 2007; *Bracken et al.*, 2013]. Frameworks built on the concept of hydrological connectivity can be useful for understanding the processes that drive landscape maintenance and evolution. For tributary systems, the hydrological connection between the channel and its floodplain plays an important role in sediment transport and deposition [*Walling et al.*, 1998; *Day et al.*, 2008; *Trigg et al.*, 2012], nutrient cycling [*Tockner et al.*, 1999; *Noe et al.*, 2013], and biodiversity and productivity [*Bornette et al.*, 1998; *Pongruktham and Ochs*, 2015]. Although hydrological connectivity in river networks is an area of active research [e.g., *Bracken and Croke*, 2007; *Ali and Roy*, 2009; *Fryirs*, 2013; *Bracken et al.*, 2013], similar work in coastal river deltas has yet to be developed. *Bracken et al.* [2013] summarize hydrological connectivity within two categories: (1) structural connectivity, which refers to the spatial arrangement of the landscape that controls patterns in flux pathways, and (2) process-based connectivity, which refers to environmental processes that produce the magnitude and direction of those fluxes. This paper investigates hydrological connectivity in river deltas by quantifying the hydrological exchange between channels and interdistributary islands (the deltaic equivalent of the tributary floodplain) and discusses its importance for delta morphology and ecology.

In recent years, an increased interest in the study of the processes controlling delta eco-geomorphology has been brought forth by a need to mitigate problems associated with coastal wetland loss [*Day et al.*, 2000, 2007], increased nutrient loading to receiving waters [*Turner and Rabalais*, 1994; *Rabalais et al.*, 2002; *Castro et al.*, 2003], anthropogenic influence [*Syvitski and Saito*, 2007; *Syvitski et al.*, 2009; *Pethick and Orford*, 2013], and other factors. Previous work on river delta surface processes has focused on one of two zones: the distributary channels or the interdistributary islands, which are the subaerial manifestation of delta structure due to sediment deposition [*Edmonds and Slingerland*, 2007; *Edmonds et al.*, 2011a]. Work on the distributary channels has primarily been concerned with the network topology [*Smart and Moruzzi*, 1972;

Morisawa, 1985; *Edmonds and Slingerland*, 2007; *Jerolmack and Swenson*, 2007; *Edmonds et al.*, 2011a; *Tejedor et al.*, 2014a, 2014b], bifurcation dynamics [*Bolla Pittaluga et al.*, 2003; *Edmonds and Slingerland*, 2007; *Sassi et al.*, 2013], mouth bar formation [*Wright*, 1977; *Edmonds and Slingerland*, 2007; *Rowland et al.*, 2010; *Mariotti et al.*, 2013], and the sediment transport within the channel and to the receiving waters [*Syvitski et al.*, 2005; *Syvitski and Saito*, 2007; *Nittrouer et al.*, 2008; *Shaw et al.*, 2013]. Within the islands, research has been concerned with island geometry [*Edmonds et al.*, 2011a; *Passalacqua et al.*, 2013], vegetation dynamics [*Neill and Deegan*, 1986; *Keddy et al.*, 2007; *Carle*, 2013], and the island biogeochemistry [*Henry and Twilley*, 2014] which has highlighted that deltaic wetlands are zones of significant denitrification able to reduce the nutrient export to receiving waters [*Lane et al.*, 1999, 2003; *DeLaune et al.*, 2005; *Yu et al.*, 2006; *Rivera-Monroy et al.*, 2010; *Henry and Twilley*, 2014]. These studies have focused on either the distributary channels or the interdistributary islands and not on the hydrological connectivity between the two. The role of process-based connectivity in coupling channel and island processes has been ignored in the literature and elements of structural connectivity between channels and islands have yet to be defined.

Hydrological connectivity is a controlling factor on the frequency and degree of inundation of delta islands, bringing water, sediment, and nutrients to the island interiors. Inundation of the interdistributary islands is a function of internal and external forces (such as riverine input, tides, and wind). Feedback mechanisms among internal dynamics of water, sediment, and nutrients play a fundamental role in deltas. As such, quantification of environmental fluxes to, within, and out of interdistributary islands under a suite of environmental forces is of a critical relevance to the understanding of processes shaping delta evolution. Furthermore, many researchers have pointed to the isolation of the channel from its floodplain due to levee construction, which can be seen as a form of hydrological (dis)connectivity [*Fryirs*, 2013], as the major factor in the acceleration of deltaic wetland degradation [*Boesch et al.*, 1994; *Day et al.*, 2000, 2007; *Paola et al.*, 2011]. Engineered river diversions have been proposed as a restoration strategy [*Kim et al.*, 2009; *Allison and Meselhe*, 2010; *Paola et al.*, 2011]. Thus, an understanding of the dynamics of hydrological connections and their associated fluxes in deltaic networks would provide a context for evaluating restored wetlands and assessing the status of vulnerable deltaic systems [*Larsen et al.*, 2012].

The goal of this study is to characterize structural and process-based connectivity in a coastal river delta by measuring water fluxes through the delta network of channels and islands at the Wax Lake Delta (WLD) in coastal Louisiana (Figure 1). The rapid formation of WLD since the 1970s with little human influence has made this delta a model for land-building river diversions in the Mississippi Delta region [*Kim et al.*, 2009; *Paola et al.*, 2011]. In order to assess the hydrological connectivity at WLD, we (1) quantify the amount of water delivered to the interdistributary islands, (2) identify internal and external drivers of flow pathways within an interdistributary island by monitoring the propagation of a hydraulic dye tracer, (3) calculate travel times through a channel-island complex, and (4) establish measures of structural and process-based connectivity in coastal river delta environments. The conclusions drawn from these analyses advance the understanding of hydrological connectivity and eco-geomorphology in coastal deltaic systems.

The remainder of the paper is structured as follows. The field site is presented in section 2 followed by a description of the instrumentation and data collection in section 3. Section 4 analyzes the velocity cross sections collected along two major distributary channels and within the interdistributary islands, the propagation of the hydraulic dye tracer released on a deltaic island, and travel times through a channel-island complex. Section 5 contains a discussion of the results in the context of hydrological connectivity and delta eco-geomorphology and presents a framework for the analysis of hydrological connectivity in coastal delta systems. We state the conclusions of this contribution in section 6.

2. Site Description

WLD is an $O(100 \text{ km}^2)$ delta located in coastal Louisiana (Figure 1) at the mouth of the 25 km long Wax Lake Outlet (WLO), which debouches into the Atchafalaya Bay about 140 km WSW of New Orleans. The WLO is a 1941 diversion dredged by the U.S. Army Corps of Engineers in an effort to reduce flooding of the Atchafalaya River [*Fisk*, 1952]. The diversion subsequently carried and deposited sediment, causing the delta to become subaerially emergent in 1973 [*Roberts et al.*, 1997]. The delta has been steadily building land since, making it one of the few deltas formed during an observable time period. Sediment input to WLD is estimated to be 38.4 Mt yr^{-1} with 18% being sand [*Kim et al.*, 2009]. Sand deposition caused most of the WLD's
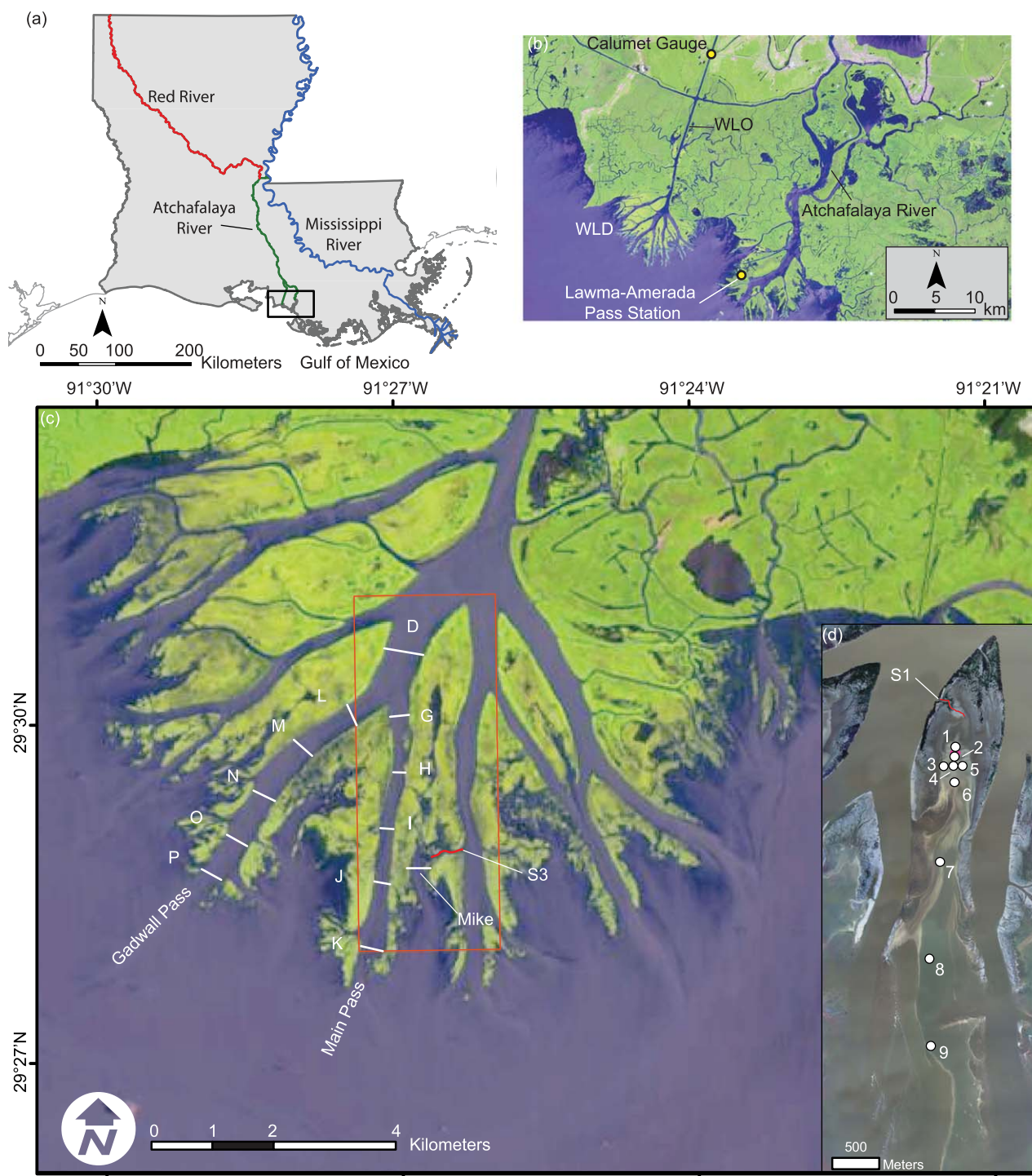
Figure 1. (a) Map of Louisiana and the major rivers contributing to the discharge at the Wax Lake Outlet (WLO) and the Wax Lake Delta (WLD). The WLO debouches into the Atchafalaya Bay at WLD and receives its discharge from the Atchafalaya River, which is fed by the Red and Mississippi Rivers. (b) The lowermost portion of the Atchafalaya River Basin. The USGS Gauge #07381590 in Calumet, LA is located about 18 km upstream of WLD along the WLO. The NOAA Lawma-Amerada Pass station (NOAA #8764227) is located in the adjacent Atchafalaya delta about 12 km ESE of the study region. (c) Map of the field measurements at Wax Lake Delta. Locations of ADCP transects traversed in Main and Gadwall Passes (16–29 June 2014) and on Mike Island (23–24 July 2012) are marked. The extent of the S3 channel has been mapped. Image specifications: LANDSAT 8 image from 19 June 2014 at 30 m resolution obtained from the USGS Global Visualization Viewer (available online at http://glovis.usgs.gov/). (d) Sensor locations for the dye tracer study performed on Mike Island from 7 to 11 February 2014. The pink hexagon between Sites 1 and 2 marks the location of the dye release point. Site S1 is the location of a secondary channel measured on 22 July 2012 and its extent has been mapped. The image is aerial photography from 6 November 2009 with 0.30 m resolution.
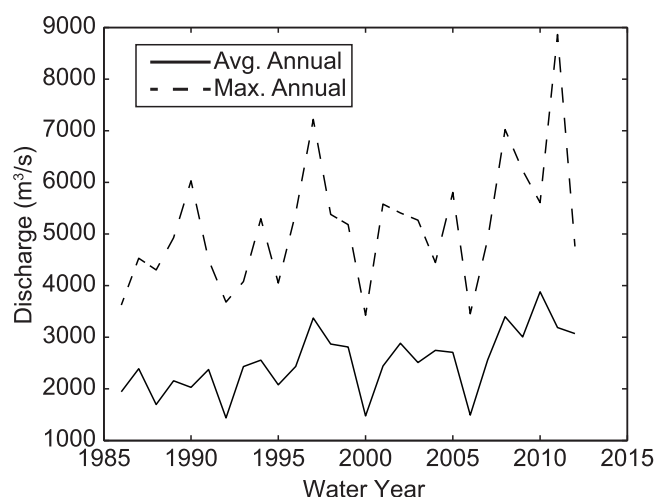
Figure 2. Average and maximum annual flows in the Wax Lake Outlet at the USGS Gauge #07381590 in Calumet, LA [*USGS*, 2014]. Average annual flows tend to be 2000–3000 m^3 s^{-1} and annual floods peak above 5000 m^3 s^{-1}.

270 mm yr^{-1} vertical accretion from 1981 to 1997 [*Edmonds et al.*, 2011a] and the deltaic deposit is estimated to be 50–70% medium sand [*Roberts et al.*, 1997]. Mixed semidiurnal microtides (average range of 0.35 m) modulate water levels on the low-gradient delta. The average annual flow in the WLO is 2500 m^3 s^{-1} and the annual flood tends to peak above 5000 m^3 s^{-1} (Figure 2). Estimates of delta progradation rate, the rate of land building, and the total subaerially exposed land obtained through remote sensing analysis [*Roberts et al.*, 2003; *Allen et al.*, 2011] and morphodynamic modeling [*Parker and Sequeiros*, 2006] are quite variable among studies. For more complete descriptions of the formation, evolution, and sedimentology of WLD, see the works of *Fisk* [1952], *Roberts et al.* [1997, 2003], and *Shaw et al.* [2013].

The WLD is composed of channels and partially inundated interdistributary islands (Figure 1). The channel network can be divided into primary (>100 m width) and secondary channels. Primary channels distribute water through the system to the Atchafalaya Bay, while secondary channels connect the primary channels to the inundated island interiors [*Shaw et al.*, 2013]. At the initial bifurcation of WLD, a large flow asymmetry exists and the downstream topology of the two branches differs greatly. The downstream topology of the eastern branch is characterized by elongated channels with relatively few bifurcations [*Edmonds et al.*, 2011a], while the western branch receives a smaller percentage of the flow and its downstream topology includes shorter channels with more bifurcations and confluences. The islands in the eastern portion tend to have greater rates of lateral and downstream migration as compared to the islands downstream of the western branch of the initial bifurcation [*Shaw et al.*, 2013]. Island levees within 4 km of the delta apex are populated with *Salix nigra* (black willow) and seem to be more stable than those without *Salix nigra* [*Shaw et al.*, 2013]. The low-relief islands are characterized by natural levees that transition from subaerial to subaqueous with increasing distance from the island apices and downstream boundaries that are open to the bay. Levees in both the subaerial and subaqueous regions are intersected by secondary channels. Near the island apices, vegetation is dense and the elevation is high in comparison to the more bayward portions of the islands, which are deeper and less vegetated.

A pictorial summary of the levee types and their relation to channel-island connectivity is presented in Figure 3. In the most upstream portions of the WLD channel network, *Salix nigra* (black willow) is present on the subaerial levees (e.g., Figure 3a). Moving downstream, the levees initially remain subaerial (e.g., Figures 1c and 3b–3f). Further downstream, both subaerial and subaqueous levees are observed, with the amount of submerged levees increasing downstream. At the channel mouths, the levees are mostly subaqueous, but less than 1 m in depth. Some of the subaqueous levees have dense vegetation (Figure 3g), while others are sparsely vegetated (Figure 3h). There are multiple secondary channels along the banks of both distributary channels (e.g., Figures 3c–3f). Secondary channels are present in the subaqueous portion as well. While these observations refer to the time and conditions at which the pictures were taken, an overall trend of increasing structural connectivity (secondary channels and subaqueous levees) moving toward the bay characterizes WLD.

3. Field Data Collection

A field campaign at WLD aimed at capturing the channel-island hydrological connectivity was composed of three trips spanning from February 2012 to June 2014. We measured (1) flow into and out of interdistributary islands via secondary channel flow, (2) the discharge along two primary channels and the allocation of water to the islands, and (3) the hydraulic behavior of an interdistributary island.

Figure 3. Examples of channel-island surface water connectivity at Wax Lake Delta. The date on which each photo was taken is in parentheses. Locations are mapped in Figure 1c. (a) East bank of transect D (19 June 2014). The vegetated subaerial bank limits hydrological connections to high water events. *Salix nigra* (black willow) line the levees in this region. (b) Mike Island subaerial vegetated levee (20 June 2012). Dense vegetation limits flow exchange over the levee top. (c) A secondary channel on the bank east of the island in the northeast corner of WLD (20 June 2014) with a vegetated flow path. (d) A secondary channel off Main Pass (18 May 2014). Vegetation within the secondary channel can limit connectivity. (e) A secondary channel with partially vegetated banks leading into Mike Island (20 June 2012). (f) A secondary channel with vegetated banks leading into the island in the northeast corner of WLD (8 May 2013). (g) A vegetated subaqueous levee near the east bank of transect J (19 June 2014). (h) The partially vegetated subaqueous levee on the east bank of transect K (19 June 2014).

Field measurements of fluxes through hydrological connections prove difficult in deltaic systems where a suite of environmental forces influence the dynamics of the system. Relatively rapid changes in water level due to tides and wind can drastically alter the connectivity at WLD (N. Geleynse et al., Identifying environmental controls on the shoreline of a natural river delta, submitted to *Journal of Geophysical Research: Earth Surface*, 2014), which is problematic when attempting to quantify connectivity measures. However, the relatively small area of WLD and the microtidal regime make WLD an ideal location to measure fluxes through hydrological connections on a system scale while controlling for water level fluctuations due to tides.

3.1. Secondary Channel and Island Discharge Measurements

Velocity transects on Mike Island (marked by transects in Figures 1c and 1d) were measured on 23–24 July 2012 during both rising and falling tides. Measurements of flow in secondary channels were made at transects S1 and S3 (Figures 1c and 1d) on 22 and 24 July, respectively, while the Mike transect (Figure 1c) was measured during both falling and rising tide on 23 July. A 2 MHz RDI StreamPro operating in water mode 12sp (a multiping version of water mode 1) [*Mueller et al.*, 2013] was towed across the transects. Each ping was composed of eight subpings and an ensemble output rate of 1 Hz was maintained. Bin sizes ranged from 0.03 to 0.10 m, depending on the maximum depth of the transect, and towing speed ranged from 0.5 to 0.9 m s^{-1}. The transducer sat 0.05 m below the water surface and had a blanking distance of 0.03 m. At least two duplicate transects were traversed at each location. The average discharge measured at the USGS gauge #07381590 [*U.S. Geological Survey (USGS)*, 2014] in Calumet, LA (18 km upstream of the WLD apex) was 1021 m^3 s^{-1} for the duration of the measurements (the discharge at the Calumet station is given for each field trip to give context, but the magnitude is not assumed to be the discharge entering the WLD apex). Water levels averaged every 6 min from the NOAA Lawma-Amerada Pass tide gauge #8764227 [*National Oceanic and Atmospheric Administration (NOAA)*, 2014] were referenced to mean lower-low water datum (MLLW) and used to relate the measured discharges to the tidal cycle.

3.2. Distributary Channel Discharge Measurements

Hydrographic surveys were performed in two major distributary channels at WLD from 16 to 19 June 2014. A boat-mounted acoustic Doppler current profiler (ADCP) measured velocity transects in both Gadwall and Main Passes. The transects were labeled "L–P" for Gadwall and "G–K" for Main (Figure 1c). Velocity transects at the feeder channel upstream of the two passes (location D) were also measured. The 2 MHz RDI StreamPro with the long-range upgrade measuring in water mode 12sp was mounted and floated from the bow of the *R/V Bluerunner*. Eight subpings comprised each ping and the data output rate was maintained at 1 Hz. The ADCP transducer sat 0.05–0.06 m below the water surface and had a blanking distance of 0.03 m. The bin size was 0.15–0.20 m, depending on the maximum depth of the transect. Boat speed averaged to about 1.0 m s^{-1}. ADCP transects were collected during both rising and falling tides, and were marked accordingly. Quadruplicate transects were traversed for each measurement, unless otherwise noted, to ensure precise results in accordance with USGS standards [*Mueller et al.*, 2013]. On average, traversing four transects took about 30 min (1800 s). To calculate discharge, the measured velocities were projected onto the average flow direction for each transect and the depth profiles to the banks were linearly extrapolated. To relate the velocity measurements with the tidal cycle, water levels were collected from the NOAA Lawma-Amerada Pass tide gauge [*NOAA*, 2014]. Average discharge from 16 to 19 June at the Calumet gauge was 3344 m^3 s^{-1} [*USGS*, 2014] and the discharge entering the WLD downstream of the initial bifurcation was 2880 m^3 s^{-1} during falling tide on 20 June.

Site selection for the discharge measurements was based on spatial and temporal feasibility. As changes in water level due to tides, river discharge, and wind may greatly alter the hydrodynamics at WLD, measurement of transects under similar conditions throughout the entire channel network is not feasible. In addition, the presence of distributary channel confluences adds considerable complexity to the measurement of discharge along the length of a primary channel. Therefore, we selected Gadwall and Main Passes due to their manageable spatial extent and because of the lack of confluences downstream of the initial bifurcation (location D in Figure 1c).

3.3. Mike Island Tracer Experiment

A dye tracer study was performed on Mike Island from 7 to 11 February 2014. Nine measurement stations were deployed in the arrangement shown in Figure 1d, which extended 3200 m longitudinally along the axis of Mike Island and spanned 200 m laterally. Sites 1, 2, and 4 were placed in intervals of 100 m

longitudinally and Sites 3 and 5 were laterally spaced 100 m from Site 4. Site 6 was 175 m south of Site 4 and Sites 7–9 were spaced at 800–1000 m intervals, depending on site conditions, along the longitudinal axis of the island. Each measurement site was equipped with a YSI 600 OMS optical rhodamine sensor (accuracy: greater of $\pm$5% reading and 1 μg L^{-1}) measuring at 45 s intervals and Sites 1, 3, 5, 7, 8, and 9 were equipped with Solinst Levelogger Junior Edges (accuracy: $\pm$10 mm) collecting a reading every 60 s. In addition, we collected wind velocity measured at 6 min intervals from the NOAA Lawma-Amerada Pass station (measured at a height of 10 m) [*NOAA*, 2014]. The average discharge at the Calumet station was 2130 m^3 s^{-1} for the duration of the experiment.

On 7 February at 15:14 CST, 1700 mL of rhodamine dye tracer was released 60 m south of Site 1 and 40 m north of Site 2. The dye was stirred at the injection point to promote vertical mixing throughout the water column. Dye propagation was observed by measurement stations until 9:40 on 11 February.

Mike Island was selected as the study location for the tracer experiment based on its potential as a hot spot for denitrification. Relatively long residence times on the relatively large and long island may promote the cycling of nitrogen [*Nixon et al.*, 1996]. A time series analysis of satellite imagery at WLD reveals that Mike Island is relatively old, which has been linked to higher organic matter content and rates of denitrification [*Henry and Twilley*, 2014].

4. Results

4.1. Hydrological Connectivity Via Secondary Channels

Flow direction in relatively small secondary channels at WLD was modulated by tides. Discharge at S1 was 0.65 m^3 s^{-1} during falling tide on 22 July 2012. The flow direction pointed out of the island (northwest), but reversed during rising tide yielding a discharge of 0.63 m^3 s^{-1} with a flow direction pointing into the island interior (southeast). The magnitudes of the discharge were essentially unchanged. At S3, the discharge was 9.90 m^3 s^{-1} during falling tide. The flow direction pointed into the island interior (west) for S3 regardless of tidal regime, supporting the notion of discharge being carried from the channels to the islands via secondary channels. With a width of about 45 m, S3 represents a relatively large secondary channel at WLD, roughly 4 times wider than S1.

4.2. Hydrological Connectivity Via Primary Channel Leakages

The results of the discharge measurements in Gadwall and Main Passes are summarized in Table 1. Discharges at the bifurcation creating Gadwall and Main Passes showed good agreement between the feeder channel (transect D) and the downstream branches (transects G and L). On 18 June during falling tide, measurements at D yielded discharges of 970 and 1126 m^3 s^{-1} separated by 1.7 h. Temporally bounded by the measurements at D, transects G and L had discharges of 277 and 779 m^3 s^{-1}, which computes to a 94–109% agreement between upstream and downstream. Similar behavior was captured on 19 June during rising tide when the discharges had a 97% agreement between D and the sum of G and L.

Figure 4 shows the downstream velocity structure for the five locations along Gadwall Pass on 18 June 2014. The figure spans a time period between falling tide until just after low tide. For each transect, the velocity core follows the thalweg of the channel and is near the surface. Maximum velocities tend to decrease moving downstream, but there are also changes due to the transition from falling to rising tide. Channel area and maximum depth decrease in the downstream direction, along with the discharge. A similar structure was observed for all of the measured transects (not shown).

Discharge measurements in Gadwall Pass on 16 June are shown in Figures 5a and 5b together with the water level at the time of each measurement. During falling tide, the average discharge at transect L-fall was 775 m^3 s^{-1}. An increase in discharge was observed when moving downstream to transect M, which had an average discharge of 836 m^3 s^{-1}. This increase was likely due to increased velocities in Gadwall Pass associated with the falling of the tide. After the measurement at transect M, a steady decline in average discharge in Gadwall Pass was observed. Transect N had an average of 725 m^3 s^{-1}, transect O had an average of 533 m^3 s^{-1}, and transect P was measured at an average of 359 m^3 s^{-1}. During rising tide, the flow at L was measured, but rough water surface conditions including waves caused inaccurate measurements. Increasing winds from the southeast (average above 3 m s^{-1}, *NOAA* [2014]) were observed during the rising tide measurements at L. The discharge exiting Gadwall Pass at transect P was 46% of that measured at

Table 1. Summary of Discharge Measurements From June 2014[a]

Time and Date	Location	Tide	Q (m^3 s^{-1})	A (m^2)	W (m)
10:30 16 Jun	L	Fall	774 (24)	1440 (69)	394 (17)
11:10 16 Jun	M	Fall	836 (11)	1348 (37)	433 (12)
12:16 16 Jun	N	Fall	725 (12)	1184 (17)	410 (9)
14:13 16 Jun	O	Rise	533 (16)	1166 (40)	403 (12)
15:14 16 Jun	P	Rise	359 (10)	1044 (90)	397 (18)
09:30 17 Jun	G	Rise	*208* (4)	*760* (13)	*359* (3)
12:12 17 Jun	G	Fall	272 (8)	746 (11)	368 (8)
12:50 17 Jun	H	Fall	268 (10)	601 (11)	222 (4)
14:03 17 Jun	I	Slack	256 (5)	602 (19)	228 (17)
14:45 17 Jun	J	Fall	254 (11)	588 (5)	269 (9)
15:42 17 Jun	K	Fall	195 (1)	614 (15)	400 (10)
16:55 17 Jun	G	Fall	279 (7)	715 (24)	376 (12)
10:22 18 Jun	D	Fall	970 (13)	2307 (30)	706 (8)
11:20 18 Jun	L	Fall	*779* (11)	*1468* (31)	*431* (7)
11:39 18 Jun	G	Fall	*277* (2)	*734* (14)	*369* (4)
12:03 18 Jun	D	Fall	*1126* (27)	*2259* (15)	*696* (5)
13:42 18 Jun	M	Slack	780 (15)	1379 (20)	462 (4)
14:45 18 Jun	N	Fall	751 (11)	1223 (21)	445 (9)
16:40 18 Jun	O	Slack	630 (16)	1157 (11)	412 (10)
17:17 18 Jun	P	Rise	*486* (9)	*1064* (48)	*397* (37)
17:42 18 Jun	L	Rise	*746* (4)	*1445* (32)	*427* (5)
08:27 19 Jun	D	Rise	*972* (12)	*2341* (28)	*714* (1)
09:07 19 Jun	G	Rise	251 (7)	747 (14)	375 (4)
09:52 19 Jun	L	Rise	698 (13)	1488 (31)	429 (19)
11:10 19 Jun	H	Slack	244 (3)	626 (13)	228 (11)
11:50 19 Jun	I	Fall	253 (4)	607 (12)	233 (8)
13:08 19 Jun	J	Fall	290 (6)	604 (24)	298 (11)
13:43 19 Jun	K	Fall	242 (6)	612 (21)	413 (8)
14:24 19 Jun	G	Fall	313 (7)	733 (21)	389 (9)

[a]Quantities are averaged among the quadruplicate transects at each location. The average computed over fewer than four transects is given in italics and values in parentheses are the standard deviations of the measurements.

L-fall. This percentage, however, does not account for the changes in discharge induced by the tide, which were measured on the second series of Gadwall Pass measurements.

On 18 June, repeat measurements were made in Gadwall Pass (Figures 5c and 5d). Little deviation in the discharge measurements at L was induced by the change in tidal regime: falling tide average discharge at L (L-fall) was 779 m^3 s^{-1}, compared to an average of 746 m^3 s^{-1} during rising tide (L-rise). Discharges downstream of L followed a similar pattern as that observed on 16 June. Transect P was measured at an average of 485 m^3 s^{-1}. When considering the change between the two discharges (falling and rising) measured at L and the average at P, 62–65% of the discharge entering at L flowed through P.

Velocity transects in Main Pass were traversed on 17 and 19 June 2014. Measurements on 17 June were performed predominantly during the falling limb of the tidal cycle (Figures 6a and 6b). The falling and low tide discharges (marked G-fall and G-low in Figure 6, respectively) were 272 m^3 s^{-1} and 279 m^3 s^{-1}, respectively. The discharge did not significantly change throughout the falling limb of the tidal cycle at this location. However, during rising tide (G-rise), the average discharge was 208 m^3 s^{-1}, which shows that tides do affect the primary channel discharges. After the G-fall measurement, discharge decreased with downstream distance, ending with an average discharge of 195 m^3 s^{-1} at transect K (Figures 6a and 6c). For the falling limb of the tidal cycle, the discharge exiting Main Pass at K was 70–72% of that entering at G (G-fall and G-low).

Figures 6c and 6d display the results from the velocity transects in Main Pass on 19 June 2014. At G, the rising (G-rise) and falling tide (G-fall) average discharges were 251 m^3 s^{-1} and 313 m^3 s^{-1}, respectively. Discharges did not steadily decrease moving downstream as measured on 17 June. This was likely due to the transects G-rise, H, and I being taken during rising tide and J, K, and G-fall being measured during falling tide. Transects H and I had discharges of 244 m^3 s^{-1} and 253 m^3 s^{-1}, respectively, and discharge increased to 290 m^3 s^{-1} at J, then dropped at K to 242 m^3 s^{-1}. This trend is in line with the measured water levels. Discharges were relatively low during rising tide at H and I, then increased at J in tandem with a decrease in water level due to falling tide. When comparing the falling tide discharges at G-fall and K, 77% was retained, which is in agreement with the observations on 17 June.
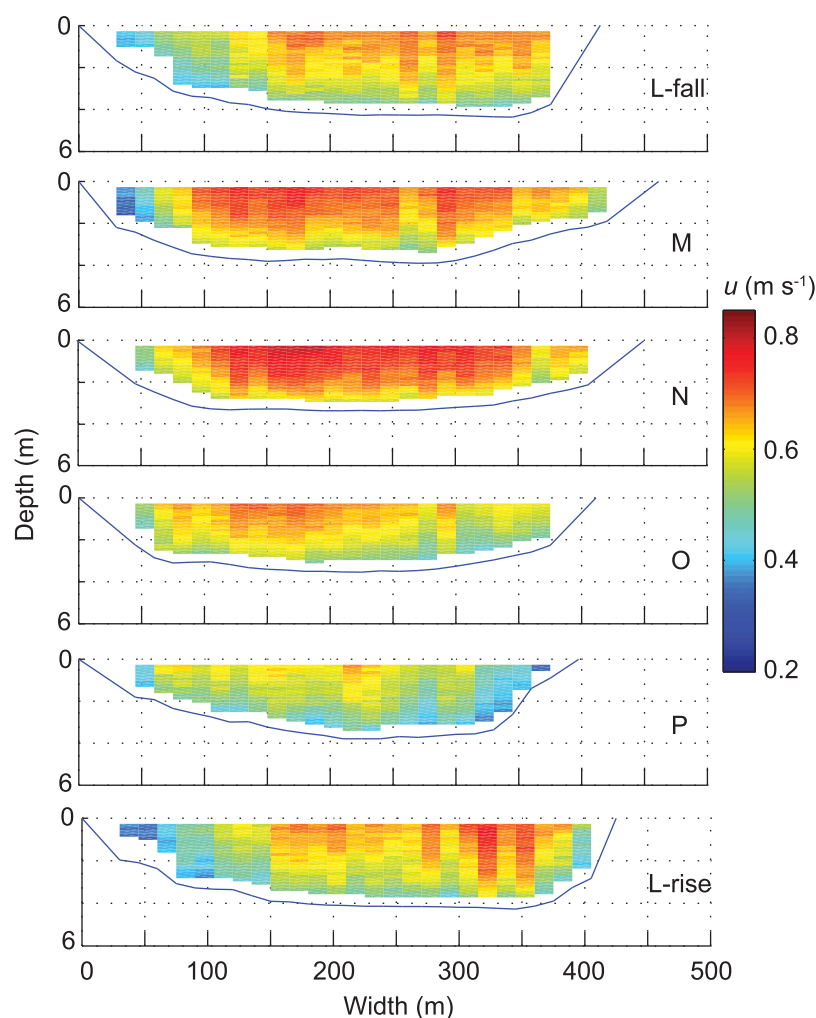
Figure 4. Spatiotemporal sequence of projected downstream velocity, u (m s^{-1}), in Gadwall Pass on 18 June 2014. The location of each transect is labeled. The bed (solid line) is linearly extrapolated to the banks. The vertical resolution of the velocity profile is 0.15 m. For visualization, the projected downstream velocity and depth profiles are horizontally binned at 15 m and averaged over repeat transects.

These results suggest that for Gadwall and Main Passes, 46–77% of the discharge entering the channel exited the mouth of the channel into the bay, indicating that a significant volume of water was delivered to the interdistributary islands (23–54%). Secondary channels and subaqueous levees likely served as conduits for flow from the channels to the inundated interdistributary islands. The reduction in flow within Gadwall and Main Passes coincided with a decrease in bank vegetation cover and a transition from subaerial to subaqueous levees (Figure 3). This channel-island surface water exchange highlights the hydrological importance of the WLD islands.

4.3. Hydraulic Behavior of an Inundated Island

After its release, the dye rapidly propagated upstream to Site 1, peaking above the detection limit of 200 μg L^{-1} (Figure 7a). Once the water levels began to fall on 7 February (Figure 7b) due to falling tide, the dye was again detected at Site 1 and subsequently Sites 2 and 4, which were located on the longitudinal axis of Mike Island directly downstream of Site 1 (Figure 1d). The plume of dye passed through Site 4 just after the higher-low tide, about 5 h after the dye was released. At the lower-high tide occurring at 22:20 CST (all subsequent times listed are CST), the dye moved back upstream and Site 4 saw an increase in rhodamine, peaking at 7.4 μg L^{-1}. About 0.3 h later, Site 2 detected rhodamine with a maximum concentration of 14.7 μg L^{-1}. The dye moved north at least 150 m during this rising limb despite the predominantly ENE winds leading up to lower-high tide (Figure 7c). Dye was also detected at Site 6 at a peak concentration of 5.6 μg L^{-1} at lower high tide. The subsequent falling tide stretching into 8 February induced a rapid downstream propagation of the plume to Sites 7, 8, and
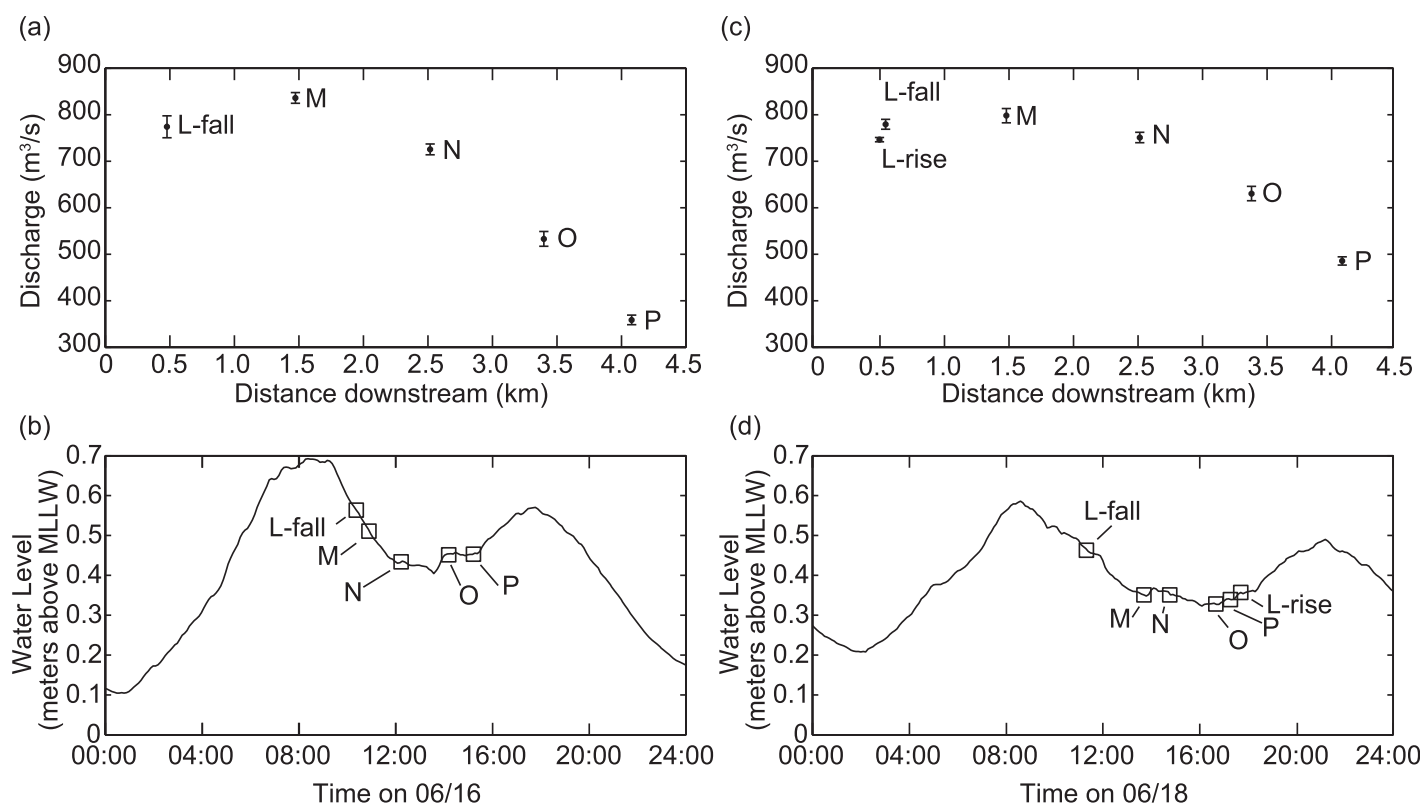
Figure 5. Discharge summary for Gadwall Pass. (top) The average discharge at each transect with the standard deviation of the measurements. (bottom) The measured water levels at the Lawma-Amerada Pass station (NOAA #8764227).

9, resulting in an average falling tide velocity from Sites 1 to 9 of 0.11 m s^{-1}. For the period of time described above, winds were less than 5 m s^{-1} from the east to east-northeast (Figure 7c).

After the low tide on 8 February, rhodamine was detected in small concentrations at Sites 1–6 and 9 at various times until high tide was reached. During this time period, wind rapidly changed direction but remained at relatively mild speeds under 5 m s^{-1}. A small peak of dye at Site 6 appeared at 18:27 on 8 February lasting about 0.5 h with a peak of 5.1 μg L^{-1}.

The next flurry of dye spikes occurred in the first half of the day on 9 February. At 1:32, a concentration averaging 3.0 μg L^{-1} passed through Site 9 in 5 min (300 s). Small concentrations were expected because of dilution and the limited spatial resolution of the sensors. About 1.5 h later at 3:04, an average of 4.5 μg L^{-1} passed through Site 8. The next detection was upstream at Site 7 at 3:53, with an average concentration of 4.5 μg L^{-1} passing through in 13 min (780 s). Time of detection from this point in time until high tide on 9 February was as follows: Site 3 at 4:49, Site 4 at 5:49, Site 6 at 6:07, Site 5 at 7:39, and at Sites 1, 2, 4, 5, 6, and 9 between 8:47 and 10:31. All locations detected rhodamine before high tide on 9 February. Winds were low during this time period, mostly less than 2.5 m s^{-1}, blowing from between ENE and ESE. No dye was detected until a similar trend in concentration readings was observed on 10 February (Figure 7a).

On 11 February, high concentrations of dye were observed in the upstream portion of the island, although there were readings at all of the sensors. Increasing winds speeds from the NE were observed before and during the morning on 11 February. As water levels fell, Site 9 detected rhodamine for 1.3 h starting at 3:05 with a peak concentration of 15.4 μg L^{-1}. Starting at 5:23, concentrations above the detection limit were measured at Sites 2 and 3 and lasted until 8:23. From 7:03 to 9:18, a steady concentration of 3.9 μg L^{-1} on average was measured at Site 4. Discrete peaks in concentration were detected at all other sites. Dye remained in the island for the duration of the experiment which lasted 3.8 days.
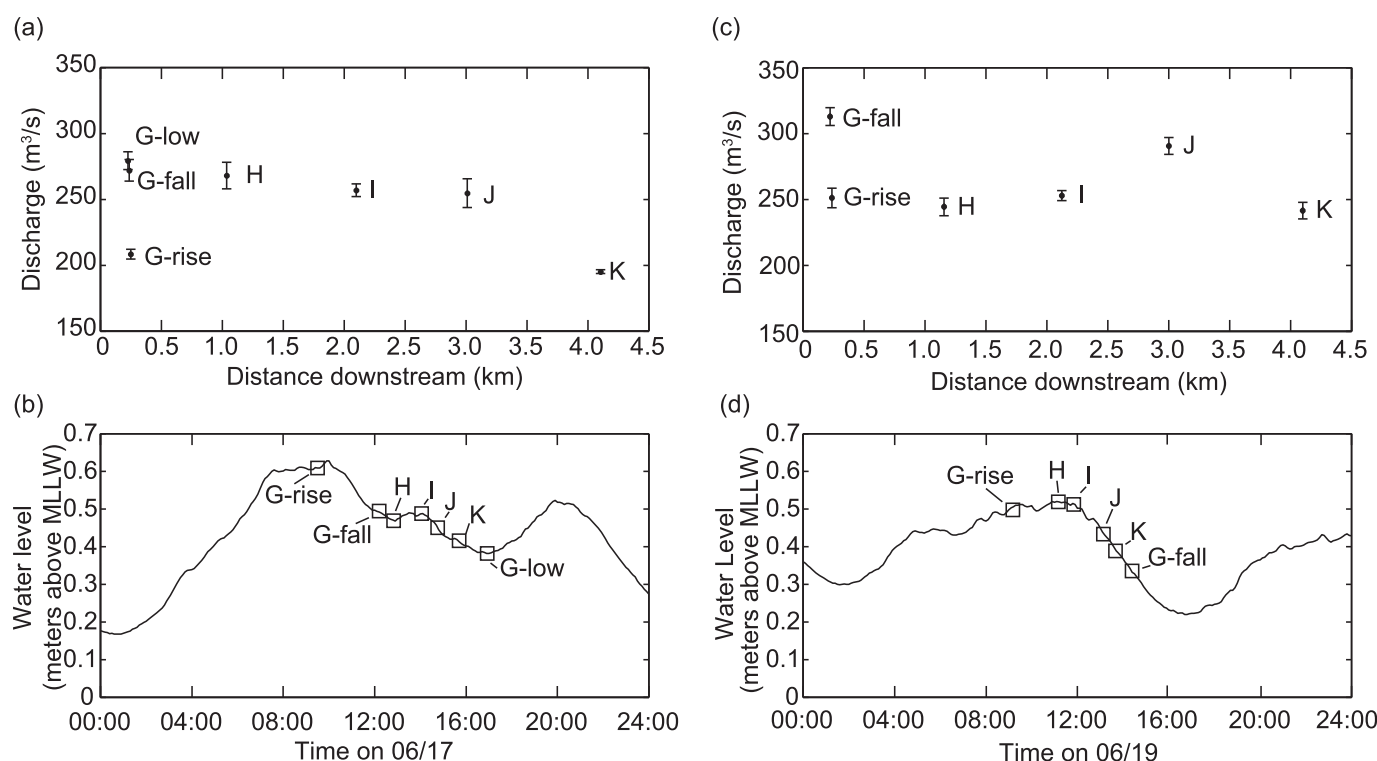
Figure 6. Discharge summary for Main Pass. (top) The average discharge at each transect with the standard deviation of the measurements. (bottom) The measured water levels at the NOAA Lawma-Amerada Pass station (NOAA #8764227).

The Mike transect velocity measurements taken in July 2012 show a reduction in average velocity from 0.14 m s^{-1} during falling tide to 0.09 m s^{-1} at rising tide. A similar reduction in velocity was observed between falling and rising tides at transects L, G, and D during the June 2014 measurements. The associated rising tide and falling tide discharges for the Mike transect were 24.7 m^3 s^{-1} and 46.2 m^3 s^{-1}, respectively. The flow exited the island to the south, toward the bay, and the direction was unaltered by the turning of the tide. Although the measured velocities were relatively low compared to those of the distributary channels, the agreement was good between the repeat measurements at the Mike transect. These results support the observed flow modulation due to tidal effects in the tracer experiment.

4.4. Travel Times Through the WLD Network

Average velocities in the channels tend to decrease moving toward the bay (Figure 4). For example, averaging over the measured transects at L-fall results in a velocity of 0.53 m s^{-1} while the average at P is 0.40 m s^{-1}. Velocities are more consistent along Gadwall Pass, but do range from 0.46 to 0.36 m s^{-1}.

To calculate the travel times of water parcels through the channel-island complexes at WLD, we consider a simple network-based approach that includes both the distributary channel and an adjacent island (Figure 8). The lengths of the channels and the island longitudinal axis are derived from the 19 June 2014 LANDSAT 8 image and the delta front bathymetry of *Shaw and Mohrig* [2014]. Channel nodes represent velocity transect measurement locations. Channel centerlines are delineated and extended to their subaqueous mouths to form the channel links while island links followed the longitudinal axis of the island. The derived geometries are assigned to each channel link along with an average falling tide velocity based on measured values at its respective upstream transect. The island is discretized similarly, with nodes being placed at the same downstream distance from transect D (Figure 1c) as their channel counterparts. Allocation of water to the islands is assumed to be symmetric, so only one island is represented in the graph (Figure 8). The island links are assigned the falling tide tracer discharge of 0.11 m s^{-1}. Therefore, this simplified model does not account for the complexity in island flows observed in the tracer study nor tidal effects and serves as a
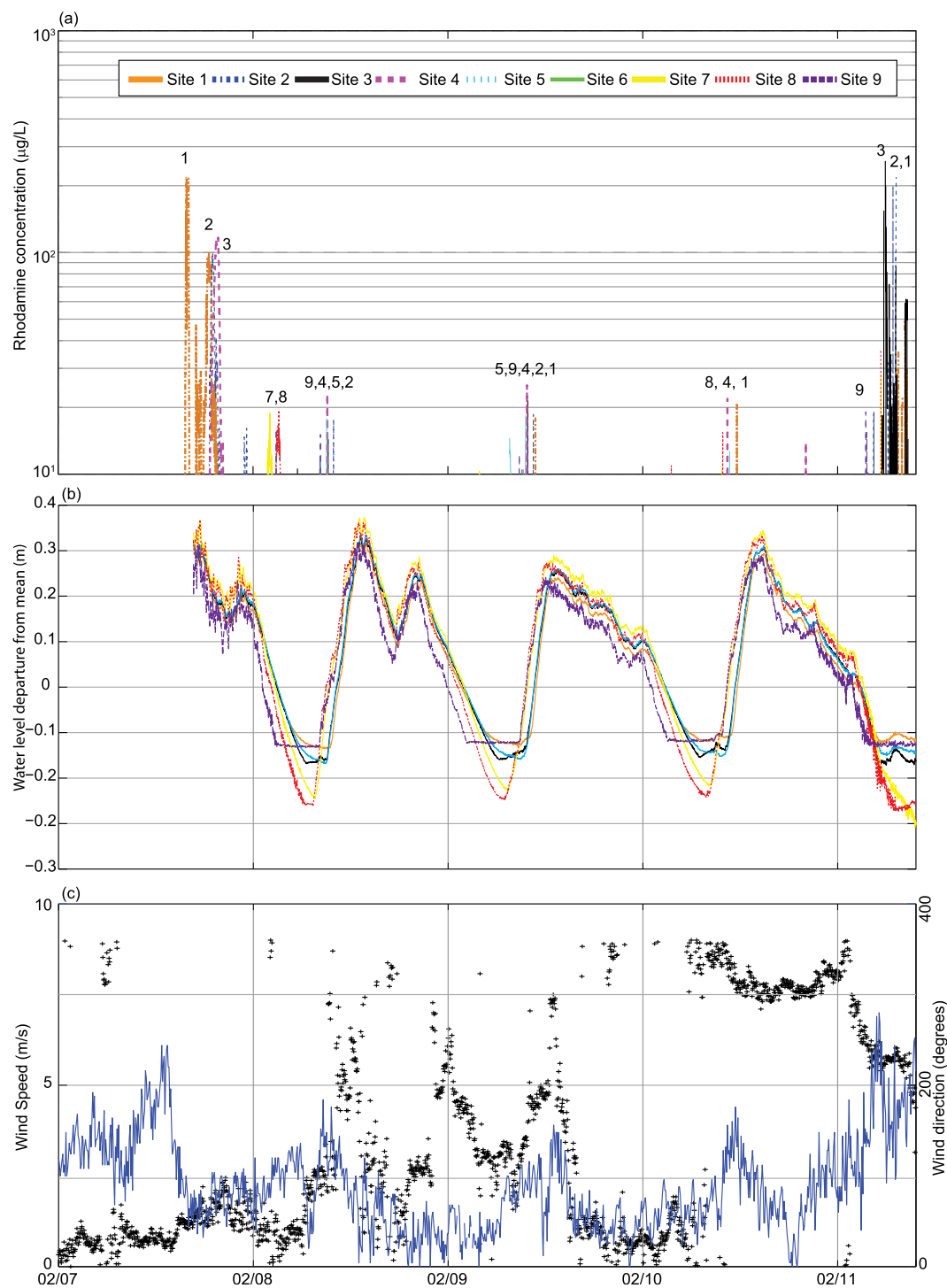
Figure 7. Summary of the tracer study performed on Mike Island in February 2014. (a) The dye concentration at each measurement location for the duration of the tracer experiment on Mike Island. Initial upstream propagation was observed after the high tide release of dye, followed by downstream movement during falling tide from late evening on 7 February to early morning on 8 February. On 11 February, a spike in concentration is observed at nearly all stations, pointing to the probable control of wind and trapping of dye by vegetation (see text for further discussion). (b) The deviation from mean water depth at Sites 1, 3, 5, 7, 8, and 9 (same color scheme as in Figure 7a). Flat areas in the troughs of the curves indicate that the water level dropped lower than the pressure transducer on the water level logger. (c) Time series of wind speed and direction measured in 6 min averages at the NOAA weather station at Lawma-Amerada Pass [*NOAA*, 2014]. The crosses indicate direction and the line represents the wind speed.
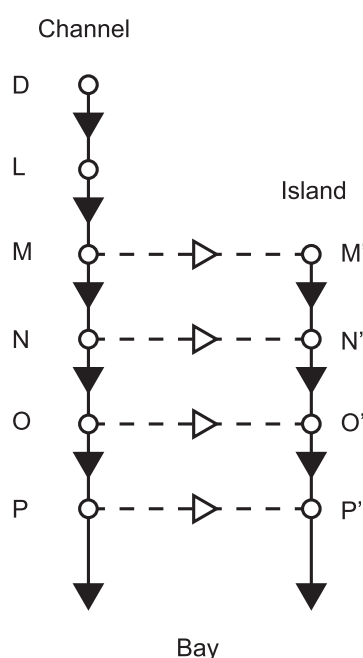
Channel

Figure 8. Travel time calculation through a channel-island complex at WLD represented here by the locations (nodes) at which measurements were taken along the channels (Figure 1c) and their island counterparts (located at the same radial distance from transect D as the channel nodes). Average velocities from the channel velocity transects and the average falling tide tracer velocity were used in the travel time calculation for the channel and island segments, respectively. In this case, the channel-island complex along Gadwall Pass is depicted.

conservative estimate of travel times of water parcels through a channel-island complex at WLD under the measured conditions. Both Gadwall and Main Passes are considered. A water parcel is allowed to enter the island downstream of transects G and L, where the allocation to the island was observed in the discharge measurements. Lateral travel times between the channel and the island were ignored.

The estimated travel times through the channel-island complex are significantly increased with water entry onto the island (Table 2). The minimum travel time of a water parcel from transect D to the bay is 4.4 h and the maximum travel time is 14.3 h, which is over 3 times the minimum. Water parcel travel times are increased by entry into the island for both Gadwall and Main Pass channel-island complexes (Table 2). The 14.3 h travel time does not include flow direction changes within the island, though water remaining on the island for this amount of time would likely be subject to tidal effects.

5. Discussion

5.1. Hydrological Connectivity in River Deltas
To summarize our hydrological connectivity analysis at WLD, a schematic depicting the flow pathways within the channel-island complex based on structural and process-based connectivity is presented in Figure 9. In the upper portion of the channel-island complex, there is limited exchange between the channel and the island interior. Secondary channels maintain the hydrological connection between the primary channel and the island interior (structural), but tidal processes control the direction of the flux (process-based). Small secondary channels (such as S1) are examples of the dynamic nature of process-based connectivity at WLD, as tides modulate flow direction. Larger secondary channels (such as S3) tend to be unidirectional because the water flux momentum tends to be greater than the momentum of tidally or wind-driven fluxes. Further downstream, the transition from subaerial to subaqueous levees promotes overbank flow from the distributary channel to the island. Gadwall and Main Passes at WLD allocated 23–54% of their water fluxes to the interdistributary islands. This suggests that substantial volumes of water at WLD are transported from the distributary channels to interdistributary islands. Surface water is carried to the island interiors from the primary channels via secondary channels and overbank flow over subaqueous levees (Figure 9). Delta islands, the recipients of this flow, are thus important portions of the hydrological network of WLD, and should, therefore, be included as part of the deltaic network for the routing of water, sediment, and nutrients. It should be noted that this overbank flow is not necessarily associated with flood discharges as in tributary systems, but was observed during relatively average riverine discharge conditions. Since water levels near the shoreline in backwater zones are relatively insensitive to discharge changes [*Chatanantavet et al.*, 2012], channel-island flow exchange is expected to persist over the range of discharges entering WLD. This mechanism of channel-island exchange is thus distinct with respect to flood-induced overbank flow in tributary systems.

Table 2. Summary of the Simplified Travel Time Calculation for the Channel-Island Complexes Along Gadwall and Main Passes (Figure 8)[a]

Path	Travel Time (h)
DLMNOP	4.4
DLMNO(P′)	8.7
DLMN(O′P′)	10.0
DLM(N′O′P′)	11.7
DL(M′N′O′P′)	13.8
DGHIJK	5.9
DGHIJ(K′)	8.6
DGHI(J′K′)	10.9
DGH(I′J′K′)	12.6
DG(H′I′J′K′)	14.3

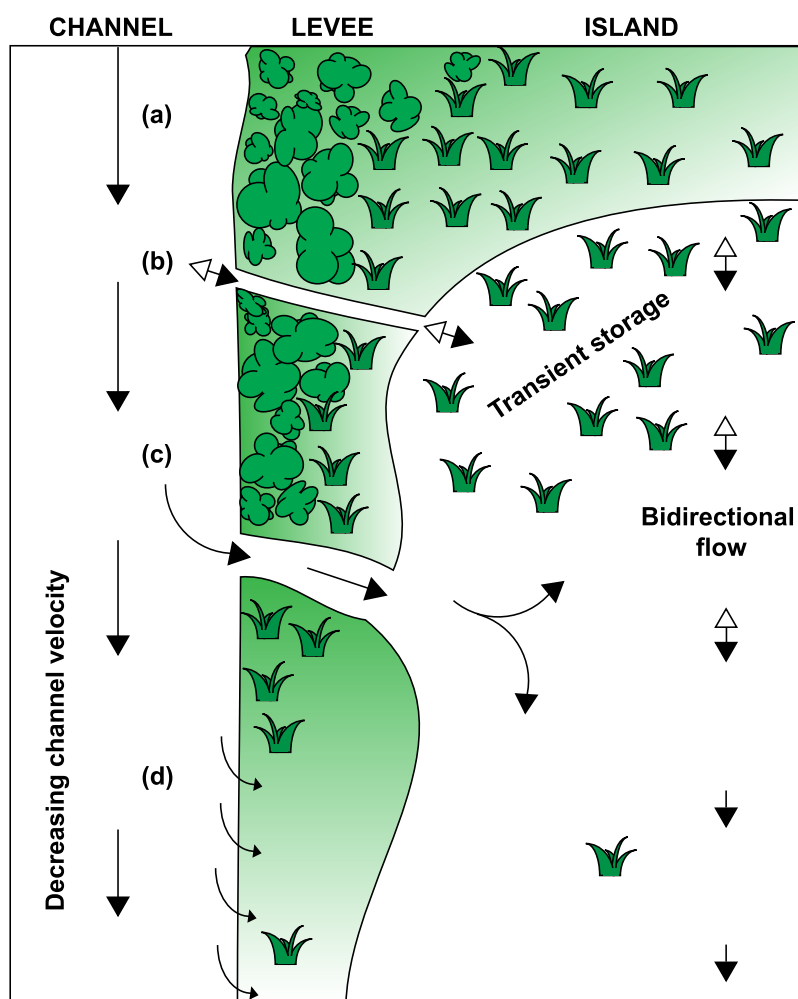[a]Locations in parentheses represent paths within the island.

Figure 9. Schematic diagram of surface water pathways for a generic and idealized channel-island complex at WLD. Flow directions are representative of the dominant flows. (a) Zone of negligible surface water connectivity between the channel and island during average flow conditions. In this region channel velocities are relatively high, the levees are heavily vegetated and subaerial, and the island interior is characterized by vegetated subaerial marshland. (b) An example of a bidirectional secondary channel which can bring flow into or out of the island interior, based on differential water level setups due to tides, wind, or riverine input. Flows in the island interior are also bidirectional, depending on the above conditions. Vegetation influences flow within the island portion of this zone (see text). (c) An example of a large unidirectional secondary channel that continually brings flow into the island. Tidal/wind induced velocities are unlikely to counteract the momentum from the channel input. (d) Zone of significant flow partitioning from the channel to the island interior. The levee zone is characterized by a transition from subaerial to subaqueous and by a decrease in vegetation. Channel velocities tend to decrease due to spreading and flow within the island interior tends to be unidirectional.

We note also that while the channel network is "distributary," and thus fluxes diverge from the apex to the bay, island fluxes converge toward the island center suggesting a "tributary" character of the island portion of the network. The channel-island network shows a mixed divergent-convergent network behavior and should be investigated in future studies on environmental transport.

Elevation is the main control on vegetation type at WLD [*Carle*, 2013], which has an effect on the hydrological connectivity between channels and islands. Near the island apices, relatively high elevation and well-established levees are populated by *Salix nigra* that stabilize the bank [*Shaw et al.*, 2013]. Hydrological connection between the primary channels and island interiors near the island apices is limited because the elevation of the banks discourages overtopping. The decrease in vegetation in the distal portion of the delta may influence the presence of secondary channels and subaqueous levees, both of which are forms of channel-island structural connectivity. The probability of significant fluxes across hydrological connections is higher in the areas with limited vegetation compared to those areas where vegetation is dense.

Figure 10. Image looking downstream taken 30 min after the rhodamine dye release on 7 February 2014. The rhodamine dye plume is bright pink due to high concentrations near the release point.

The direction of flow within the island is controlled by the tide, the magnitude of flux from the primary channel, and wind. Surface water within the island is slow moving and is populated by emergent vegetation. In areas receiving little flux from the primary channels, wind and tides exert significant effects on the flow dynamics because the ambient water has little momentum input from the channel. For example, upstream propagation of the dye was observed during the rising limb of the tidal cycle directly after injection and dye returned upstream during the next rising limb (Figure 7), which points to the control of tides. Increased winds likely have caused the large spikes in dye concentration on 11 February (Figure 7). The northeast winds may have released dye in transient storage within vegetation patches (Figure 10) in the northern portion of the island near Sites 1, 2, 3, and 4, leading to high concentrations of dye being sporadically released from transient storage. The upstream portion of the island responds to the tidal cycle and wind events. Tidal momentum, however, may not be able to reverse flow directions near large secondary channels or in the presence of overbank flow. Upstream tidal amplification and spatial differences in island water depths may also play a role in determining where flow inversion due to tides occurs. These observations support the introduction of hydrological connectivity into the study of river deltas. Complex behavior driven by several external drivers, as well as the internal complexity of the system, necessitate system-scale observations that can be analyzed within the context of hydrological connectivity.

Tidal action affects discharge within the distributary channels by lowering velocities during rising tide and increasing them during the falling limb. Rising tide discharges were 74–96% of their falling tide counterparts and no effect on flow direction was detected in our observations. The discharge at transect Mike during rising tide was 53% of the falling tide discharge and the bayward flow direction was unchanged. Secondary channels may instead exhibit flow inversion, depending on topographic and environmental conditions. Channel S1, characterized by a small discharge, exhibited a flow inversion. Channel S3 carried a larger discharge and consistently flowed into the islands regardless of tidal regime. The secondary channel flows were measured during a period of very low flow (1021 m^3 s^{-1} measured upstream at Calumet) and the relatively small river forcing may have enhanced the effect of the tides.

Because of the large spatial domain of Mike Island and the limited spatial resolution of the sensors, dye likely entered unmeasured portions of the island or followed pathways circumventing the sensor locations. Velocities on the island are small and thus the dye tracer was likely weakly mixed in the transverse direction. The significance of the tracer study does not hinge on lateral mixing, as the convergent nature of the island fluxes likely contained the bulk of the tracer to the island longitudinal axis, where our sensors were located, which allowed the behavior of the dye to be measured.

This study does not address the groundwater component of hydrological connectivity. Hyporheic flow across the levee likely comprises a portion of the discharge reduction observed in the distributary channels. This study also ignores the effects of the spring and neap tide and significant changes in riverine input. These factors should be addressed in future studies.

5.2. Implications to Delta Morphology
The presence of significant hydrological connections between the primary channels and interdistributary islands at WLD has important implications for delta evolution both morphologically and ecologically. As

water flows into the islands at WLD, it carries sediment and nutrients. We argue that this hydrological connection is of first-order importance to delta eco-geomorphic evolution.

The allocation of flow to WLD islands suggests that hydrological connectivity between channels and islands (or floodplains) influences delta morphology, as the delivery of sediment via water flow is crucial for developing and maintaining delta form [*Edmonds et al.*, 2011a]. Since the primary channels at WLD can be erosional [*Edmonds et al.*, 2011b; *Shaw et al.*, 2013; *Shaw and Mohrig*, 2014], deposition within the islands is important for the maintenance of the delta platform. During large floods, which likely increase channel-island connectivity, sand is transported in suspension [*Shaw et al.*, 2013] and can deposit on the subaqueous island interiors [*Shaw and Mohrig*, 2014]. During below-average flows, sand is deposited on the levees, while channels extend and bifurcations remain stable [*Shaw and Mohrig*, 2014]. The significant water flux to islands facilitates sediment transport to island levees and interiors. Thus, increased connectivity to deltaic floodplains may provide a possible avenue for mitigating wetland loss. Various investigators have proposed increasing channel-floodplain connectivity through engineered river diversions [*Day et al.*, 2000; *Kim et al.*, 2009; *Allison and Meselhe*, 2010; *Paola et al.*, 2011]. Of such implemented diversions, the West Bay diversion in Louisiana has been shown to retain 30–70% of the sediment supplied, leading to subaerial land formation [*Kolker et al.*, 2012]. A system-scale analysis of hydrological connectivity is a vital piece in understanding the evolution of natural deltas and engineered river diversions.

The water flux to the islands decelerates the channel flow due to spreading and friction, which decreases the momentum of the channel flow. This has important implications for the prediction of delta distributary network structure. The slowing of velocities due to flow expansion in a turbulent jet has been identified as the driving process in the development of river mouth bars [*Wright*, 1977; *Edmonds and Slingerland*, 2007; *Mariotti et al.*, 2013] and subaqueous levees [*Rowland et al.*, 2010]. At WLD, the expansion of flow is occurring over several kilometers as water is fluxed over subaqueous levees and, thus, may not rapidly expand like a turbulent plane jet in a standing body of water. The overbank flux may favor subaqueous levee formation over mouth bar formation [*Rowland et al.*, 2010], which would lead to the elongated channel pattern observed in the east-central portion of WLD [*Edmonds et al.*, 2011a] since sand can be deposited on levees during low-flow conditions [*Shaw and Mohrig*, 2014]. Since centerline velocity exhibits an effect on the distance to a river mouth bar [*Edmonds and Slingerland*, 2007], the effect of water flux to islands must be accounted for in models for predicting bifurcation length scales. Due to the complexity of the problem, modeling studies often treat distributary channel mouths as turbulent jets with no overbank flow upstream of the mouth [e.g., *Edmonds and Slingerland*, 2007], but future work should include this condition of upstream overbank flow.

5.3. Implications to Delta Ecology

At the landscape level, hydraulic travel times through aquatic systems are relatively unknown in coastal settings [*Rivera-Monroy et al.*, 2010], but are essential to the prediction of denitrification at large scales [*Yu et al.*, 2006; *Rivera-Monroy et al.*, 2010]. At WLD, we have quantified the travel times of water parcel through a channel-island complex by including the islands in the hydrological network, which significantly increases travel times. Currently, WLD contains few islands that tend to be relatively large [*Edmonds et al.*, 2011a]. As river deltas grow according to river mouth bar models, bifurcation distance decreases with increasing distance from the delta apex [*Edmonds and Slingerland*, 2007; *Jerolmack and Swenson*, 2007], creating a large number of smaller islands. As islands grow and more are formed, fluxes from the primary channels into the islands will increase travel times as more island area is available for transport of material. Island sizes in a mature delta have been shown to have a power-law distribution [*Passalacqua et al.*, 2013], which may lead to a heavy-tailed distribution of travel times.

High concentrations of nitrate are present in the Mississippi and Atchafalaya River waters [*Rivera-Monroy et al.*, 2010; *Lane et al.*, 2011] and ambient concentrations in WLD have been measured at >60 μM [*Henry and Twilley*, 2014]. Since a significant portion of the water at WLD enters the islands, nitrate transport to the islands is likely significant as well. The connectivity between channels and islands represents an important ecological link at WLD that may modulate nitrate cycling. In the Davis Pond river diversion near WLD, *Yu et al.* [2006] modeled $42 \pm 2.5\%$ and $95 \pm 0.5\%$ nitrate removal for travel times of 1 and 5 days, respectively. These results provide a context for understanding the ecological impact of travel times at WLD. For the case of transport exclusively by primary channels from transect D to the bay, travel times are in the order of a

few hours (Table 2), which indicates that denitrification in channels is likely limited by the travel time at WLD. However, the tracer study revealed that dye remained in the system after 3.8 days. Increased travel times associated with water parcels entering islands within the channel-island complex model (Table 2) and the tracer result suggests that significant denitrification may occur when nitrate is transported to the islands.

6. Conclusions

In this study, we have quantified the surface water component of hydrological connectivity between distributary channels and interdistributary islands at WLD over tidal time scales and related that exchange to delta evolution and environmental transport. We find that a significant portion of the WLD water flux passes through the interdistributary island interiors and that travel times within the islands are controlled by a suite of environmental forces, which subsequently influence system travel times. The conclusions we draw from the analyses of flow partitioning and island hydrologic pathways at WLD provide new insight into channel-island coupled processes in river deltas, linking for the first time distributary channels and interdistributary islands, previously analyzed as separate entities at different spatial and temporal scales. We find this coupling to be fundamental to delta eco-geomorphic evolution. The results of this work can be used to validate predictive models of environmental transport in natural river deltas and engineered river diversions.

Transects surveyed with a boat-mounted ADCP along two distributary channels at WLD were used to quantify the volumetric water exchanged with interdistributary islands over tidal time scales during relatively average upstream discharge conditions. The ADCP was also used to measure flows within secondary channels connecting the primary channels to an island interior and the discharges exiting the bayward boundaries of an island. A hydraulic dye tracer was deployed on an inundated island in the delta network to quantify the hydraulic residence time and to characterize the flow of the island interior subject to wind and tidal forces. A simplified model of a channel-island complex was used to calculate travel times. From analyses of these data, we make the following conclusions:

1. Interdistributary islands have a significant hydrological connection with distributary channels and play an important role in the hydrological network at WLD. Discharge measurements within primary channels indicate that 46–77% of the water flux at the initial bifurcation is conveyed to the bay. The remaining discharge (23–54%) is allocated to the interdistributary islands, which indicates that islands deliver a volume of water to the bay that is on the same order of magnitude as the distributary channels. Secondary channels and overbank flow over subaqueous levees act as the avenues for the channel-island connectivity and vegetation likely plays a role in determining the spatial distribution of flow exchange. Channels consistently allocate water to the islands regardless of the tidal regime for the measured upstream flow conditions. Since the islands convey significant discharge to the receiving waters, network analyses of WLD and similar deltas must include the inundated interiors of islands and their connections to the major distributary channels in order to appropriately represent the hydrological behavior of the system. Ignoring islands as part of the delta network would result in a reduction of fluxes measured at the system outlet and anomalously short travel times. For example, at WLD, ignoring islands would result in 23–54% less flux to the bay and at least 3 times shorter travel times through the system.

2. Tides affect the process-based connectivity of surface water between the distributary channels and islands at WLD. Flow into and out of the islands is modulated by the tidal cycle. However, since flow exchange was observed regardless of the tidal regime, structural connectivity in the form of secondary channels and flow over subaqueous levees controls the flow exchange at WLD. Discharges exiting the bayward boundaries of an interdistributary island were reduced by the rising tide to 53% of the falling tide discharge. In a small secondary channel, the tide modulated the flow direction, but the flow direction in a large secondary channel was unaltered.

3. Water flux into the island interiors increases the time for a water parcel to travel through the WLD network. Travel times calculated with a simplified model of water transport through a channel-island complex range from 4.4 to 14.3 h, depending on flow path. A dye tracer experiment revealed dye was present in high concentrations 3.8 days after the release of the dye, which points to the complex hydraulic behavior of the island interiors and potential for increased travel times for water entering the interdistributary islands. The significant allocation of water to the islands and the increased travel times enhance the denitrification potential of deltaic systems such as WLD.

References

Ali, G. A., and A. G. Roy (2009), Revisiting hydrologic sampling strategies for an accurate assessment of hydrologic connectivity in humid temperate systems, *Geogr. Compass*, 3(1), 350–374, doi:10.1111/j.1749-8198.2008.00180.x.

Allen, Y., B. Couvillion, and J. Barras (2011), Using multitemporal remote sensing imagery and inundation measures to improve land change estimates in coastal wetlands, *Estuaries Coasts*, 34(1), 190–200, doi:10.1007/s12237-011-9437-z.

Allison, M. A., and E. A. Meselhe (2010), The use of large water and sediment diversions in the lower Mississippi River (Louisiana) for coastal restoration, *J. Hydrol.*, 387(34), 346–360, doi:10.1016/j.jhydrol.2010.04.001.

Boesch, D. F., M. N. Josselyn, A. J. Mehta, J. T. Morris, W. K. Nuttle, C. A. Simenstad, and D. J. P. Swift (1994), Scientific assessment of coastal wetland loss, restoration and management in Louisiana, *J. Coastal Res.*, special issue 20, 1–103.

Bolla Pittaluga, M., R. Repetto, and M. Tubino (2003), Channel bifurcation in braided rivers: Equilibrium configurations and stability, *Water Resour. Res.*, 39(3), 1046, doi:10.1029/2001WR001112.

Bornette, G., C. Amoros, and N. Lamouroux (1998), Aquatic plant diversity in riverine wetlands: The role of connectivity, *Freshwater Biol.*, 39(2), 267–283, doi:10.1046/j.1365-2427.1998.00273.x.

Bracken, L. J., and J. Croke (2007), The concept of hydrological connectivity and its contribution to understanding runoff-dominated geomorphic systems, *Hydrol. Processes*, 21(13), 1749–1763, doi:10.1002/hyp.6313.

Bracken, L., J. Wainwright, G. Ali, D. Tetzlaff, S. Smith, S. Reaney, and A. Roy (2013), Concepts of hydrological connectivity: Research approaches, pathways and future agendas, *Earth Sci. Rev.*, 119, 17–34, doi:10.1016/j.earscirev.2013.02.001.

Carle, M. (2013), Spatial structure and dynamics of the plant communities in a pro-grading river delta: Wax Lake Delta, Atchafalaya Bay, Louisiana, PhD thesis, La. State Univ., Baton Rouge, La.

Castro, M., C. Driscoll, T. Jordan, W. Reay, and W. Boynton (2003), Sources of nitrogen to estuaries of the United States, *Estuaries*, 26(3), 803–814, doi:10.1007/BF02711991.

Chatanantavet, P., M. P. Lamb, and J. A. Nittrouer (2012), Backwater controls of avulsion location on deltas, *Geophys. Res. Lett.*, 39, L01402, doi:10.1029/2011GL050197.

Day, G., W. E. Dietrich, J. C. Rowland, and A. Marshall (2008), The depositional web on the floodplain of the Fly River, Papua New Guinea, *J. Geophys. Res.*, 113, F01S02, doi:10.1029/2006JF000622.

Day, J., Jr., L. Britsch, S. Hawes, G. Shaffer, D. Reed, and D. Cahoon (2000), Pattern and process of land loss in the Mississippi Delta: A spatial and temporal analysis of wetland habitat change, *Estuaries*, 23(4), 425–438, doi:10.2307/1353136.

Day, J., Jr., et al. (2007), Restoration of the Mississippi Delta: Lessons from Hurricanes Katrina and Rita, *Science*, 315, 1679–1684, doi:10.1126/science.1137030.

DeLaune, R., A. Jugsujinda, J. West, C. Johnson, and M. Kongchum (2005), A screening of the capacity of Louisiana freshwater wetlands to process nitrate in diverted Mississippi River water, *Ecol. Eng.*, 25(4), 315–321, doi:10.1016/j.ecoleng.2005.06.001.

Edmonds, D., C. Paola, D. Hoyal, and B. Sheets (2011a), Quantitative metrics that describe river deltas and their channel networks, *J. Geophys. Res.*, 116, F04022, doi:10.1029/2010JF001955.

Edmonds, D., J. B. Shaw, and D. Mohrig (2011b), Topset-dominated deltas: A new model for river delta stratigraphy, *Geology*, 39(12), 1175–1178, doi:10.1130/G32358.1.

Edmonds, D. A., and R. L. Slingerland (2007), Mechanics of river mouth bar formation: Implications for the morphodynamics of delta distributary networks, *J. Geophys. Res.*, 112, F02034, doi:10.1029/2006JF000574.

Fisk, H. (1952), Geological Investigation of the Atchafalaya Basin and the Problem of Mississippi River Diversion, U.S. Army Corps. of Eng., Miss. River Comm., Vicksburg, Miss.

Fryirs, K. (2013), (Dis)connectivity in catchment sediment cascades: A fresh look at the sediment delivery problem, *Earth Surf. Processes Landforms*, 38(1), 30–46, doi:10.1002/esp.3242.

Henry, K., and R. Twilley (2014), Nutrient biogeochemistry during the early stages of delta development in the Mississippi River deltaic plain, *Ecosystems*, 17(2), 1–17, doi:10.1007/s10021-013-9727-3.

Jerolmack, D., and J. Swenson (2007), Scaling relationships and evolution of distributary networks on wave-influenced deltas, *Geophys. Res. Lett.*, 34, L23402, doi:10.1029/2007GL031823.

Keddy, P., D. Campbell, T. McFalls, G. Shaffer, R. Moreau, C. Dranguet, and R. Heleniak (2007), The wetlands of Lakes Pontchartrain and Maurepas: Past, present and future, *Environ. Rev.*, 15(1), 43–77.

Kim, W., D. Mohrig, R. Twilley, C. Paola, and G. Parker (2009), Is it feasible to build new land in the Mississippi River Delta?, *Eos Trans. AGU*, 90(42), 373–374.

Kolker, A. S., M. D. Miner, and H. D. Weathers (2012), Depositional dynamics in a river diversion receiving basin: The case of the West Bay Mississippi River Diversion, *Estuarine Coastal Shelf Sci.*, 106, 1–12, doi:10.1016/j.ecss.2012.04.005.

Lane, R., J. W. Day, and B. Thibodeaux (1999), Water quality analysis of a freshwater diversion at Caernarvon, Louisiana, *Estuaries*, 22(2), 327–336, doi:10.2307/1352988.

Lane, R., H. Mashriqui, G. Kemp, J. Day, J. Day, and A. Hamilton (2003), Potential nitrate removal from a river diversion into a Mississippi delta forested wetland, *Ecol. Eng.*, 20, 237–249, doi:10.1016/S0925–8574(03)00043-0.

Lane, R., C. Madden, J. Day, and D. Solet (2011), Hydrologic and nutrient dynamics of a coastal bay and wetland receiving discharge from the Atchafalaya River, *Hydrobiologia*, 658, 55–66, doi:10.1007/s10750-010-0468-4.

Larsen, L., J. Choi, M. Nungesser, and J. W. Harvey (2012), Directional connectivity in hydrology and ecology, *Ecol. Appl.*, 22, 2204–2220, doi:10.1890/11–1948.1.

Mariotti, G., F. Falcini, N. Geleynse, M. Guala, T. Sun, and S. Fagherazzi (2013), Sediment eddy diffusivity in meandering turbulent jets: Implications for levee formation at river mouths, *J. Geophys. Res. Earth Surf.*, 118, 1908–1920, doi:10.1002/jgrf.20134.

Morisawa, M. (1985), Topologic properties of delta distributary networks, in *Models in Geomorphology*, edited by M. J. Woldenberg, pp. 239–268, Allen and Unwin, St. Leonards, NSW, Australia.

Mueller, D., C. Wagner, M. Rehmel, K. Oberg, and F. Rainville (2013), Measuring discharge with acoustic Doppler current profilers from a moving boat (ver. 2.0, December 2013), *U.S. Geol. Surv. Tech. Methods*, Book 3, Chap. A22, 95 pp. [Available at http://pubs.usgs.gov/tm3a22/.].

Neill, C., and L. A. Deegan (1986), The effect of Mississippi River Delta lobe development on the habitat composition and diversity of Louisiana coastal wetlands, *Am. Midland Nat.*, 116(2), 296–303.

Nittrouer, J. A., M. A. Allison, and R. Campanella (2008), Bedform transport rates for the lowermost Mississippi river, *J. Geophys. Res.*, 113, F03004, doi:10.1029/2007JF000795.

Nixon, S., et al. (1996), The fate of nitrogen and phosphorus at the land-sea margin of the North Atlantic Ocean, *Biogeochemistry*, *35*, 141–180, doi:10.1007/BF02179826.

NOAA (2014), National Oceanic and Atmospheric Administration (NOAA) Tides and Currents. [Available at http://tidesandcurrents.noaa.gov/, last accessed 1 Jul 2014.]

Noe, G., C. Hupp, and N. Rybicki (2013), Hydrogeomorphology influences soil nitrogen and phosphorus mineralization in floodplain wetlands, *Ecosystems*, *16*(1), 75–94, doi:10.1007/s10021-012-9597-0.

Paola, C., R. Twilley, D. Edmonds, W. Kim, D. Mohrig, G. Parker, E. Viparelli, and V. Voller (2011), Natural processes in delta restoration: Application to the Mississippi Delta, *Ann. Rev. Mar. Sci.*, *3*, 67–91, doi:10.1146/annurev-marine-120709–142856.

Parker, G., and O. Sequeiros (2006), Large scale river morphodynamics: Application to the Mississippi delta, in *River Flow 2006: Proceedings of the International Conference on Fluvial Hydraulics*, edited by R. Ferreira et al. 3–11, Taylor and Francis, London, U. K.

Passalacqua, P., S. Lanzoni, C. Paola, and A. Rinaldo (2013), Geomorphic signatures of deltaic processes and vegetation: The Ganges-Brahmaputra-Jamuna case study, *J. Geophys. Res. Earth Surf.*, *118*, 1838–1849, doi:10.1002/jgrf.20128.

Pethick, J., and J. D. Orford (2013), Rapid rise in effective sea-level in southwest Bangladesh: Its causes and contemporary rates, *Global Planet. Change*, *111*, 237–245, doi:10.1016/j.gloplacha.2013.09.019.

Pongruktham, O., and C. Ochs (2015), The rise and fall of the Lower Mississippi: Effects of hydrologic connection on floodplain backwaters, *Hydrobiologia*, *742*(1), 169–183, doi:10.1007/s10750-014-1983-5.

Rabalais, N., R. Turner, and W. Wiseman Jr. (2002), Gulf of Mexico hypoxia, A.K.A. The Dead Zone, *Ann. Rev. Ecol. Syst.*, *33*, 325–363, doi:10.1146/annurev.ecolsys.33.010802.150513.

Rivera-Monroy, V., P. Lenaker, R. Twilley, R. Delaune, C. Lindau, W. Nuttle, E. Habib, R. Fulwiler, and E. Castaneda-Moya (2010), Denitrification in coastal Louisiana: A spatial assessment and research needs, *J. Sea Res.*, *63*, 157–172, doi:10.1016/j.seares.2009.12.004.

Roberts, H., R. Cunningham, G. Kemp, and S. Majersky (1997), Evolutions of sedimentary architecture and surface morphology: Atchafalaya and Wax Lake Deltas, Louisiana (1973–1994), *Gulf Coast Assoc. Geol. Soci. Trans.*, *47*, 477–484.

Roberts, H., J. Coleman, S. Bentley, and N. Walker (2003), An embryonic major delta lobe: A new generation of delta studies in the Atchafalaya-Wax Lake Delta system, *Gulf Coast Assoc. Geol. Soci. Trans.*, *53*, 690–703.

Rowland, J. C., W. E. Dietrich, and M. T. Stacey (2010), Morphodynamics of subaqueous levee formation: Insights into river mouth morphologies arising from experiments, *J. Geophys. Res.*, *115*, F04007, doi:10.1029/2010JF001684.

Sassi, M. G., A. J. F. Hoitink, B. Vermeulen, and H. Hidayat (2013), Sediment discharge division at two tidally influenced river bifurcations, *Water Resour. Res.*, *49*, 2119–2134, doi:10.1002/wrcr.20216.

Shaw, J., and D. Mohrig (2014), The importance of erosion in distributary channel network growth, Wax Lake Delta, Louisiana, USA, *Geology*, *42*, 31–34, doi:10.1130/G34751.1.

Shaw, J., D. Mohrig, and S. Whitman (2013), The morphology and evolution of channels on the Wax Lake Delta, Louisiana, USA, *J. Geophys. Res. Earth Surf.*, *118*, 1562–1584, doi:10.1002/jgrf.20123.

Smart, J., and V. Moruzzi (1972), Quantitative properties of delta channel networks, *Z. Geomorphol.*, *16*(3), 283–300.

Syvitski, J., and Y. Saito (2007), Morphodynamics of deltas under the influence of humans, *Global Planet. Change*, *57*, 261–282, doi:10.1016/j.gloplacha.2006.12.001.

Syvitski, J., et al. (2009), Sinking deltas due to human activities, *Nat. Geosci.*, *2*, 681–686, doi:10.1038/ngeo629.

Syvitski, J. P., A. J. Kettner, A. Correggiari, and B. W. Nelson (2005), Distributary channels and their impact on sediment dispersal, *Mar. Geol.*, *222–223*, 75–94, doi:10.1016/j.margeo.2005.06.030.

Tejedor, A., A. Longjas, I. Zaliapin, and E. F. Georgiou (2014a), Delta channel networks. 1: A graph-theoretic approach for connectivity analysis and steady-state flux solutions, *Water Resour. Res.*, in press.

Tejedor, A., A. Longjas, I. Zaliapin, and E. F. Georgiou (2014b), Delta channel networks. 2: Metrics of topologic and dynamic complexity for delta comparison, physical inference and vulnerability assessment, *Water Resour. Res.*, in press.

Tetzlaff, D., C. Soulsby, P. J. Bacon, A. F. Youngson, C. Gibbins, and I. A. Malcolm (2007), Connectivity between landscapes and riverscapes—A unifying theme in integrating hydrology and ecology in catchment science?, *Hydrol. Processes*, *21*(10), 1385–1389, doi:10.1002/hyp.6701.

Tockner, K., D. Pennetzdorfer, N. Reiner, F. Schiemer, and J. V. Ward (1999), Hydrological connectivity, and the exchange of organic matter and nutrients in a dynamic riverfloodplain system (Danube, Austria), *Freshwater Biol.*, *41*(3), 521–535, doi:10.1046/j.1365–2427.1999.00399.x.

Trigg, M. A., P. D. Bates, M. D. Wilson, G. Schumann, and C. Baugh (2012), Floodplain channel morphology and networks of the middle Amazon River, *Water Resour. Res.*, *48*, W10504, doi:10.1029/2012WR011888.

Turner, R., and N. Rabalais (1994), Coastal eutrophication near the Mississippi River Delta, *Nature*, *368*, 619–621, doi:10.1038/368619a0.

USGS (2014), U.S. Geological Survey (USGS) Water Data for the Nation. [Available at http://waterdata.usgs.gov/nwis/, last accessed 20 Jun 2014.]

Walling, D. E., P. N. Owens, and G. J. Leeks (1998), The role of channel and floodplain storage in the suspended sediment budget of the River Ouse, Yorkshire, UK, *Geomorphology*, *22*(34), 225–242, doi:10.1016/S0169–555X(97)00086-X.

Wright, L. (1977), Sediment transport and deposition at river mouths: A synthesis, *Geol. Soc. Am. Bull.*, *88*, 857–868.

Yu, K., R. DeLaune, and P. Poeckx (2006), Direct measurement of denitrification activity in a Gulf coast freshwater marsh receiving diverted Mississippi River water, *Chemosphere*, *65*, 2449–2455, doi:10.1016/j.chemosphere.2006.04.046.